BIOCHEMISTRY
including biophysical chemistry & molecular biology
Article

*Biochemistry* **2010,** *49,* 9063–9071 9063
DOI: 10.1021/bi100516e

# Compound Ice-Binding Site of an Antifreeze Protein Revealed by Mutagenesis and Fluorescent Tagging[†]

Christopher P. Garnham,[‡] Aditya Natarajan,[‡] Adam J. Middleton,[‡] Mike J. Kuiper,[§] Ido Braslavsky,[∥] and Peter L. Davies*,[‡]

[‡]*Department of Biochemistry, Queen's University, Kingston, Ontario, Canada K7L 3N6,* [§]*Victorian Partnership for Advanced Computing, Carlton South, Victoria 3053, Australia, and* [∥]*Department of Physics and Astronomy, Ohio University, Athens, Ohio 45701, USA*

*Received April 6, 2010; Revised Manuscript Received September 17, 2010*

ABSTRACT: By binding to the surface of ice crystals, type III antifreeze protein (AFP) can depress the freezing point of fish blood to below that of freezing seawater. This 7-kDa globular protein is encoded by a multigene family that produces two major isoforms, SP and QAE, which are 55% identical. Disruptive mutations on the ice-binding site of type III AFP lower antifreeze activity but can also change ice crystal morphology. By attaching green fluorescent protein to different mutants and isoforms and by examining the binding of these fusion proteins to single-crystal ice hemispheres, we show that type III AFP has a compound ice-binding site. There are two adjacent, flat, ice-binding surfaces at 150° to each other. One binds the primary prism plane of ice; the other, a pyramidal plane. Steric mutations on the latter surface cause elongation of the ice crystal as primary prism plane binding becomes dominant. SP isoforms naturally have a greatly reduced ability to bind the prism planes of ice. Mutations that make the SP isoforms more QAE-like slow down the rate of ice growth. On the basis of these observations we postulate that other types of AFP also have compound ice-binding sites that enable them to bind to multiple planes of ice.

Many organisms that inhabit ice-laden environments produce antifreeze proteins (AFPs)[1] to protect themselves from potentially lethal *in vivo* ice growth (*1*−*3*). By binding to the surface of seed ice crystals, the AFPs stop their growth and lower the nonequilibrium freezing point of a solution below the melting point (i.e., noncolligative freezing point depression) (*4*). Adsorption of AFPs to the ice surface also slightly raises the melting temperature (*5*, *6*). Typically, the difference between the depressed freezing point and the melting point is termed thermal hysteresis (TH) and is used as a measure of antifreeze activity (*7*). However, it is more precise to define TH as the difference between the depressed freezing point and the raised melting point. In other words, TH is the sum of the freezing and melting hystereses (FH + MH).

AFPs display a remarkable diversity in sequence and structure (*8*−*15*). However, despite obviously divergent origins, all AFPs have evolved the ability to bind to ice and halt its growth (*16*, *17*). AFPs are thought to stop the growth of ice via an adsorption−inhibition mechanism (*4*) whereby ice is forced to grow between bound AFPs in energetically unfavorable curved fronts that cause a lowering of the freezing point by the Kelvin effect (*18*). This prevents ice growth within the TH gap until the temperature of the solution is lowered sufficiently to breach the inhibition by bound AFPs, leading to rapid and uncontrolled ice crystal growth.

There are many distinct planes of ice (defined by Miller indices) that present different patterns of oxygen atoms on their surfaces. This has been suggested to account for some of the diversity in AFP structures (*16*). Original ice-etching studies performed using type I AFP from winter flounder and Alaskan plaice identified the pyramidal plane {20−21} as the surface bound on the ice crystal (*18*). Subsequently, ice etches of the hyperactive spruce budworm AFP (sbwAFP) (*9*) showed simultaneous prism and basal plane binding. The explanation offered for this was that the basal and primary prism planes of ice have very similar spacing of oxygen atoms, therefore allowing the regular array of Thr residues that constitute the ice-binding site (IBS) of the protein to interact with both surfaces. A more complex ice-binding situation was observed with fish type III AFP when ice-etching studies revealed the protein's affinity toward both the primary prism and a pyramidal plane of ice (*19*). This corrected an earlier study where just the primary prism plane was identified as the binding surface for type III AFP (*20*, *21*). The idea that a single AFP might have affinity toward multiple ice planes has been largely unexplored in the antifreeze field, but multiplane binding might be the rule rather than the exception.

Type III AFP is a 7-kDa globular protein found in fish that inhabit both Arctic and Antarctic waters (*22*). The protein is typically produced *in vivo* as a mixture of SP-Sephadex and QAE-Sephadex binding isoforms (*23*). Amino acid sequence identity within each group is high (ca. 90% for SP isoforms, 75% for QAE isoforms) while identity between SP and QAE isoforms is lower (ca. 55%). Structures of both the SP and QAE isoforms have been determined (*10*, *24*−*27*). The IBS of the protein has been identified through several site-directed mutagenesis studies and is located on a flat, relatively hydrophobic area of the protein (*28*−*32*). Its location on the protein is supported by

[†]This research was funded by a grant to P.L.D. from the Canadian Institutes for Health Research (CIHR). P.L.D. holds a Canada Research Chair in Protein Engineering. C.P.G. is the recipient of an NSERC PGSD3 scholarship.

*To whom correspondence should be addressed. Phone: (613) 533-2983. Fax: (613) 533-2497. E-mail: peter.davies@queensu.ca.

[1]Abbreviations: AFP, antifreeze protein; FIPA, fluorescence-based ice plane affinity; GFP, green fluorescent protein; IBS, ice-binding site; IPTG, isopropyl β-D-1-thiogalactopyranoside; nfe, notched fin eelpout; Ni-NTA, nickel nitrilotriacetic acid; NMR, nuclear magnetic resonance; op, ocean pout; PVC, polyvinyl chloride; QAE, quaternary aminoethyl; SDS−PAGE, sodium dodecyl sulfate−polyacrylamide gel electrophoresis; SP, sulfopropyl; TH, thermal hysteresis; Tris, tris(hydroxymethyl)aminomethane; UV, ultraviolet.


Published on Web 09/20/2010

recent solid-state NMR experiments (*33*) that identified a cluster of residues (amino acid positions 10−20) that exhibited pronounced side-chain chemical shift changes upon freezing, indicative of ice binding. Ice crystals typically adopt a hexagonal bipyramidal shape in the presence of type III AFP. A mutation series substituting residue Ala16 on the IBS of the protein with increasingly bulkier amino acids resulted in incrementally lower TH levels, with the mutation A16H being the most deleterious (25% of wild-type activity) (*31*). The A16H mutation never completely arrested ice growth during the TH measurements. Video recordings showed the crystal grew at a steady rate into a highly elongated hexagonal bipyramid. The loss of TH activity of this mutant has been correlated with disturbances of the ice-like pattern of hydrating water molecules on the IBS (*34*).

Recently, a family of 13 type III AFP homologues was described in the notched fin eelpout *Zoarces elongatus* Kner (*35*). They fit into the QAE and SP isoform series, and the QAE isoforms were further subdivided into QAE1 and QAE2 sets. All recombinantly expressed QAE isoforms had some level of TH activity, but recombinant versions of two SP isoforms (termed nfeAFP2 and nfeAFP6) were unable to stop ice growth. They each shaped ice into hexagonal bipyramids typical of type III AFP, but steady growth of the bipyramids was observed throughout TH measurements. Interestingly, ice growth could be arrested by adding a small amount of "active" QAE isoform to a solution of "inactive" SP isoform (*35*, *36*). This phenomenon of ice-shaping without TH activity by an SP isoform of type III AFP has been observed before (*37*) and is similar to that produced by the A16H mutant previously mentioned.

In this paper, the structural basis for the altered ice-binding and ice-shaping abilities of the type III AFP A16H mutant and nfeAFP6 SP isoform has been investigated via fluorescence-based ice plane affinity (FIPA) analysis. By fusing GFP to type III AFP (*38*) and growing large single-crystal ice hemispheres, a major improvement in the convenience of the ice-etching method (*19*) has been made possible and has allowed for visualization of bound protein on the hemisphere under UV light. This study has confirmed that type III AFP can indeed bind multiple planes of ice and that the inability of both the A16H mutant and the notched fin eelpout (nfe) SP isoform to stop ice growth correlates with decreased surface coverage of the ice crystal. Also, a double mutation made to the "inactive" nfe SP isoform helped convert it into an "active" QAE-like isoform of type III.

## EXPERIMENTAL PROCEDURES

*Cloning and Site-Directed Mutagenesis*. The genes encoding QAEop12 and QAEop_A16H were originally cloned into the pT7-7f vector (*39*). PCR amplification of both genes was performed using primers that introduced an N-terminal *Nde*I cut site and a C-terminal *Xho*I cut site. Each gene was ligated into the *Nde*I/*Xho*I sites of the pET24a expression vector (Novagen), thereby adding a C-terminal hexahistidine tag. The gene encoding SPnfe6 was synthesized by GENEART Inc. (http://www.geneart.com). An N-terminal *Nde*I cut site and C-terminal *Xho*I cut site were built into the synthetic gene to allow for ligation into the *Nde*I/*Xho*I sites of pET24a after its removal from the supplied pMA vector. This again placed a C-terminal hexahistidine tag on the protein. The gene encoding GFP (purchased from Clontech and supplied in the pEGFP vector) was PCR amplified using primers that placed *Nde*I cut sites at the N and C termini of the gene. The GFP gene PCR product was ligated upstream of all the AFP clones into the *Nde*I cut site of the pET24a vector and checked for the correct orientation. A three-residue Gly-Ala-Gly linker was present between the GFP and AFP. The QuickChange multisite-directed mutagenesis kit (Stratagene) was used to create the SPnfe6_P19L/A20V double mutant. All positive clones were verified by restriction digestion followed by DNA sequencing (Robarts Research Institute, London, Ontario, Canada).

*Protein Expression and Purification*. Positive clones were expressed in the *Escherichia coli* BL21 DE3 Star cell line (Invitrogen). Cultures (1 L) were grown at 37 °C with shaking until the $OD_{600nm}$ = 0.5, then transferred to a 23 °C shaking incubator, and allowed to grow to an $OD_{600nm}$ = 1.0. Protein expression was induced by the addition of IPTG to a final concentration of 1 mM and allowed to continue overnight at 23 °C with shaking. Cells were pelleted by centrifugation at 3500 rpm in a Beckman Coulter JA4.2 rotor and were resuspended in 25 mL of buffer N (50 mM Tris-HCl (pH 8.0), 500 mM NaCl, 5 mM imidazole, 100 $\mu$M PMSF) and lysed via sonification using a model 500 sonic dismembrator (Fisher Scientific). The lysate was spun at 16000 rpm in a Beckman Coulter JA25.5 rotor, and the lysate supernate was brought to 200 mL in buffer N containing 5 mL of Ni-NTA agarose resin (Qiagen). The mixture was stirred for 20 min at room temperature. The resin was washed with 2 column volumes of buffer N prior to protein elution using buffer N containing 400 mM imidazole. The Ni-NTA eluate was dialyzed overnight against 10 mM Tris-HCl (pH 8.0). The purity of the Ni-NTA eluate was determined by SDS−PAGE in a 10% (w/v) gel. The dialyzed eluate was used for ice-binding experiments with the single-crystal ice hemispheres. All constructs not fused to GFP underwent an additional purification procedure where the Ni-NTA eluate was further fractionated by gel permeation chromatography using a G-75 column (Amersham Biosciences) equilibrated in 50 mM Tris-HCl (pH 8.0) and 200 mM NaCl. Protein concentration was determined by UV absorbance using the protein's extinction coefficient as predicted by ProtParam (http://ca.expasy.org/tools/protparam.html).

*Tetramethylrhodamine Labeling of SPnfe6*. A 500 $\mu$L sample of SPnfe6 (10 mg/mL) was dialyzed against 100 mM $NaHCO_3$ (pH 8.5) after which 50 $\mu$L of 10 mg/mL tetramethylrhodamine (product no. T6105, Invitrogen) was added. The sample was allowed to rotate at room temperature for 3 h. Labeled protein was separated from unincorporated label by passing the sample through a 5 mL 5-kDa molecular mass cutoff dextran desalting column (Thermo Scientific) equilibrated in 10 mM $NaHCO_3$ (pH 8.5) and collected as the flow-through.

*Single-Crystal Hemispheres*. Single ice crystals were grown in a metal pan placed floating in a temperature-controlled ethylene glycol bath. The pan contained sections of PVC pipe roughly 4 cm in diameter by 4 cm in height sealed to the bottom of the pan by vacuum grease. These acted as molds for the growth of single ice crystals. However, as one reviewer has pointed out, since PVC releases ice-active substances that can modify ice growth habit and interfere with ice recrystallization, it would be prudent to use a different plastic for this purpose. On the bottom surface of each pipe section was a tiny notch (1 mm wide × 1 mm high × 4 mm long) that allowed for water entry/ice growth. Distilled, degassed $H_2O$ was poured into the pan to a depth of 0.8 cm and entered the PVC molds through their notch. The temperature of the ethylene glycol bath was initially set at −0.5 °C, and once the $H_2O$ had supercooled to that temperature, ice nucleation was induced by addition of a piece of multicrystalline ice to the center of the pan. Ice growth in the PVC molds occurred

only once it had reached the notched entry. Once ice had sealed the bottom of the molds, degassed $H_2O$ was added to each casing on top of the ice layer, and the temperature was lowered in 0.2 °C increments until the entire casing was frozen (typically 1 week later). Ice disks were removed from their molds and viewed under cross-polarized light to ensure they were single crystals with no defects and to identify the crystallographic basal plane (normal to the crystal's optical axis). The crystal was then wrapped in aluminum foil, poked with a needle in the basal plane, and allowed to sublimate for 15 min in a lyophilizer. Doing so produced a hexagonal pattern on the basal plane of the crystal that identified the primary and secondary prism planes of the crystal (*40*). Crystals of known orientation were mounted on the coldfinger by melting a hole in the top of the crystal in the same shape as the end of the brass rod. The coolant in the coldfinger was initially set to −0.5 °C and then immediately reduced to −4 °C upon attachment of the ice crystal. The crystal was then immersed in ca. 30 mL of 10 mM Tris-HCl (pH 8.0) and allowed to melt back into a hemispherical shape. At this point, ca. 2−3 mL of buffer was removed and replaced with an equal volume of a particular GFP-AFP construct in the same buffer, with a final protein concentration of 0.1−0.2 mg/mL. The temperature of the coolant was lowered to −7 °C, and the hemisphere was allowed to grow for 4−5 h, allowing for inclusion of the GFP-AFP construct into a newly deposited ice layer on the hemisphere that was 1−3 mm in thickness. These conditions are very similar to those used in developing a conventional ice etch (*9*, *18*). The fluorescence signal was checked with a hand-held UV light. The hemisphere was removed from the brass finger and viewed at 4 °C under UV light using a DyNA light dual intensity UV transilluminator (National Labnet Co.). Images of the hemispheres were taken using a Canon SD300 digital camera. Hemispheres can be stored at −20 °C prior to, and after, imaging.

*TH Measurements*. TH measurements and ice crystal images were made as previously described (*41*, *42*). TH measurements were performed in buffer containing 10 mM Tris-HCl (pH 8.0). All ice growth rate measurements were recorded at a temperature 0.05 °C below the equilibrium melting temperature of the solution.

## RESULTS

*GFP-Tagged QAE Isoform of Type III AFP Binds to Multiple Planes of Ice*. GFP fused to the N terminus of wild-type HPLC12, a QAE type III AFP from ocean pout (referred to as GFP-QAEop12), was produced at levels of >10 mg/L of *E. coli* culture. It was soluble and was approximately 90% pure following Ni-NTA chromatography as judged by SDS−PAGE analysis (data not shown). A single-crystal ice hemisphere mounted with its secondary prism plane normal to the coldfinger (Figure 1A) was immersed in a dilute solution (~0.1 mg/mL) of GFP-QAEop12 and allowed to grow until its diameter had increased by 1−3 mm. The fluorescence signal is proportional to the thickness of this added layer, and it is possible, though unnecessary, to accumulate a layer of new ice that is even thicker without spoiling the definition of the ice-binding planes by the increased fluorescence. At this point a broad patch of fluorescence covering the entire equatorial area (relative to the vertical *c*-axis) of the hemisphere was seen (Figure 1B). The fluorescent patch consisted of two symmetrical lobes whose junction is inclined at roughly 10° with respect to the *c*-axis of the ice crystal. The complexity and pattern of the fluorescence with respect to

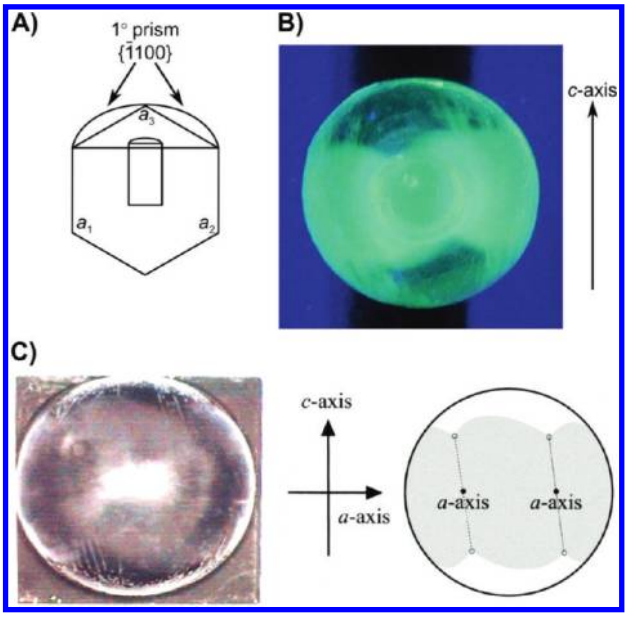


FIGURE 1: Binding of GFP-tagged QAEop12 to an ice hemisphere. (A) The single-crystal ice hemisphere was mounted so that the secondary prism plane was normal to the long axis of the coldfinger. The directions of the crystallographic *a*-axes are indicated, as are the Miller indices of the primary prism planes (in braces). (B) Resulting fluorescent pattern of bound QAEop12 viewed under UV light. The view (looking down an *a*-axis) is normal to the view in panel A. The basal planes of the crystal are at the top and bottom of the image and show no bound protein. (C) Shown for comparison is the original type III AFP etch and its interpretation published by Antson et al. (*19*).

the orientation of the crystal is highly suggestive of more than one ice plane being bound. Our interpretation is that the underlying two distinct lobes of fluorescence correspond to primary prism plane binding while the overlapping pattern and its rotation with respect to the *c*-axis suggest affinity toward an unspecified pyramidal plane. No fluorescence was observed in the areas corresponding to the basal planes of the crystal (the top and bottom of the crystal as viewed in Figure 1B). This matches the etch obtained by the traditional method with recombinant QAE type III AFP (Figure 1C) (*19*), except that the crystal in our experiment was mounted normal to a secondary prism plane and not a primary prism plane. This explains why only two lobes are observed in this experiment vs the three previously seen by Antson et al. (*19*). Our results confirm the original observations of these authors that this AFP binds to more than one plane of ice while validating that GFP tagging does not change the mode of AFP binding.

*A Steric Mutation on the AFP Simplifies the Ice-Binding Footprint*. A similar experiment was performed using the A16H mutant of QAEop12 (referred to as QAEop12_A16H), one of the most severely affected activity mutants identified in a study by Deluca et al. (*30*). In this previous study, QAEop12_A16H shaped ice into hexagonal bipyramids with an increased *c*:*a* axial ratio as compared to wild type and was unable to stop ice growth during TH measurements. The hemisphere (mounted as in the wild-type experiment) obtained with the fluorescently tagged mutant showed a large decrease in surface coverage (Figure 2A) as compared to that with GFP-QAEop12 (Figure 1B). Two distinct patches of fluorescence were observed on the hemisphere, and the location of these patches was consistent with primary prism plane binding. Each patch was rotated with respect to the *c*-axis at a ca. 45° angle . This angle differs from the 10° angle

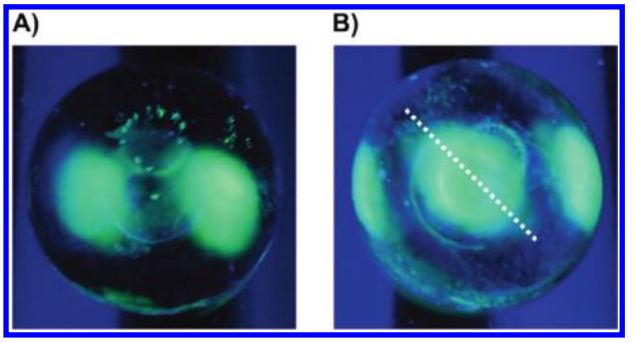


FIGURE 2: Binding of GFP-tagged QAEop12_A16H to an ice hemisphere. (A) The hemisphere was mounted with the coldfinger normal to a secondary prism plane. Two distinct patches of fluorescence can be seen that correspond to primary prism plane binding. (B) Fluorescent hemisphere mounted normal to a primary prism plane. Three distinct patches of fluorescence can be seen that again correspond to primary prism plane binding. The hatched white line indicates the direction of rotation of the patches with respect to the *c*-axis of the ice crystal.

observed on the hemisphere of GFP-QAEop12; however, 10° is simply the apparent junction angle between the overlapping fluorescent lobes on the hemisphere and not the actual rotation of each lobe with respect to the *c*-axis of the crystal. Not until the decreased surface coverage produced by the A16H mutant of QAEop12 resolved the overlapping fluorescent lobes into discrete patches could the angle of rotation of each patch with respect to the *c*-axis of the crystal be more accurately determined. Indeed, each fluorescent lobe on the hemisphere produced by GFP-QAEop12 also appears to be rotated at a ca. 45° angle as well. No basal or pyramidal plane binding was observed. Another hemisphere was grown with its primary prism plane normal to the ice finger, and it showed three distinct patches of fluorescence instead of two (Figure 2B). This further highlights the decreased surface coverage of the hemisphere by this mutant as compared to the wild type and confirms that the primary prism plane of ice is the main and possibly only surface to which QAEop12_A16H is able to bind.

*An SP Isoform Has Compromised Ice-Binding Ability*. Since replacement of A16 by a bulky residue (His) caused both the loss of TH activity (*30*) and a simplification of the ice hemisphere fluorescence pattern, we elected to see if a TH-inactive isoform of type III AFP also had a simplified ice-binding pattern. We chose SPnfe6, an SP isoform of type III AFP produced by the notched fin eelpout, because it has been well documented that this isoform cannot stop the growth of an ice crystal, although it does shape ice into a hexagonal bipyramid (*35*). GFP was fused to SPnfe6 to analyze its ice-binding ability. The surface coverage of the hemisphere was dramatically reduced as compared to GFP-QAEop12 (Figure 3), even more so than the GFP-QAEop12_A16H hemisphere. Two conspicuous patches of fluorescence were seen on the hemisphere. Each patch consisted of two distinct lobes located above and below the equator of the hemisphere that were joined together by a small section of fluorescence. Since the hemisphere was mounted with its secondary prism plane normal to the ice finger, and due to the 2-fold symmetry of each lobe with respect to the equatorial *a*-axes of the crystal, the lobes of each fluorescent patch represent affinity toward a pyramidal plane of unspecified Miller indices, with the linker between the two indicating a small amount of primary prism plane binding. While both pyramidal and prism planes are bound, they are covered to a much lesser extent as compared to GFP-QAEop12.

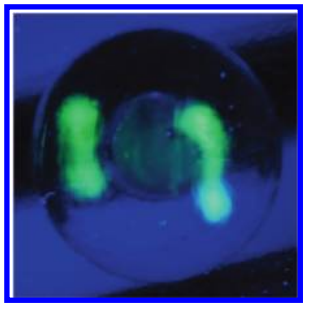

FIGURE 3: Binding of GFP-tagged SPnfe6 to an ice hemisphere. The hemisphere was mounted with its secondary prism plane normal to the coldfinger. Two distinct patches of fluorescence can be seen, with the lobes in each patch corresponding to pyramidal plane binding and the small patch of fluorescence linking each lobe being the signature for primary prism plane binding.

*A Double Mutation to SPnfe6 Increases Ice-Binding Activity*. Amino acid alignment between SPnfe6 and QAEop12 shows a high degree of conservation of the 12 putative ice-binding residues (boxed in Figure 4), with two main exceptions. At amino acid positions 19 and 20, SPnfe6 contains proline and alanine, respectively, while QAEop12 contains leucine and valine, respectively. A double substitution of P19L/A20V was made to SPnfe6 in order to probe the significance of these residues with respect to ice binding. The double mutant was also fused to GFP for FIPA analysis. With the GFP-tagged double mutant, a broad patch of fluorescence was observed across the entire surface of the hemisphere (Figure 5), similar to that produced by QAEop12 (Figure 1B). The hemisphere was mounted with its primary prism plane normal to the ice finger, and three distinct lobes were present within the fluorescence oriented in the same manner as seen in Figure 1. The increased surface coverage produced by this double mutation, which is similar to that produced by QAEop12, suggested that the mutant protein would have TH activity and not just be able to shape ice crystals into hexagonal bipyramids.

*TH Activity and Ice-Shaping Activity of SPnfe6 and SPnfe6_P19L/A20V*. The genes for both SPnfe6 and SPnfe6_P19L/A20V were cloned without GFP to produce the proteins for accurate TH measurements and the determination of ice-crystal morphology and growth rates. Both proteins were produced in good yield and were purified via Sephadex G-75 size-exclusion and Ni-NTA chromatographies. Each protein was pure following this procedure as deemed by SDS−PAGE analysis (data not shown). As previously mentioned, SPnfe6 is unable to stop ice growth during undercooling situations (*35*). This phenomenon was confirmed as can be seen in the time lapse images of an ice crystal in a 100 $\mu$M solution of SPnfe6 held at 0.05 °C below the melting point of the solution (Figure 6). The crystal grew at a rate of 12.7 $\mu$m/min (Table 1). This growth rate is similar to that previously reported for this protein (*36*). However, the rate of growth in our study was determined by measuring the length of the crystal from tip to tip along the *c*-axis and not the width along the *a*-axes as was done by Takamichi et al. (*36*). This produced a higher growth rate by a factor of the crystal length over width and allowed for more accurate measurements of the growth rate. In contrast, QAEop12 was able to completely stop ice crystal growth (Table 1).

The ice shaping and TH activities of SPnfe6_P19L/A20V were then tested. At a concentration of 100 $\mu$M, the double mutant lowered the ice crystal growth rate to 0.4 $\mu$m/min, which is a greater than 30-fold decrease as compared to SPnfe6 at the same concentration (Table 1). Images of an ice crystal after 1 and 15 min can be

```
QAEop12    MNQASVVANQLIPINTALTLVMMRSEVVTPVGIPAEDIPRLVSMQVNRAVPLGTTLMPDMVKGYA-A   66
              **** **********  **  ++  * ***  ++ +++*   ***  *  * **** *** ++ *
SPnfe6       GESVVATQLIPINTALTPAMMEGKVTNPSGIPFAEMSQIVGKQVNTPVAKGQTLMPGMVKTYVPAK   66
```

FIGURE 4: Amino acid alignment between QAEop12 and SPnfe6. Identical residues between the two proteins are represented by *, while + represents a conserved substitution. Residues thought to be involved in ice binding are boxed.

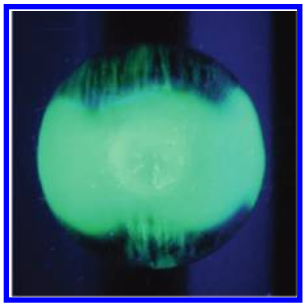

FIGURE 5: Binding of GFP-tagged Spnfe6_P19L/A20V to an ice hemisphere. The hemisphere was mounted with its primary prism plane normal to the ice finger.

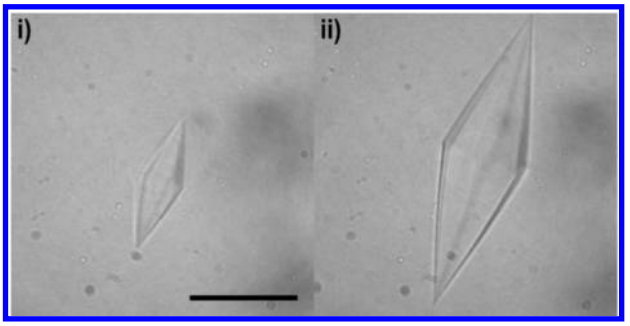


FIGURE 6: Ice crystal morphology and growth in the presence of SPnfe6. Images of an ice crystal in 100 $\mu$M SPnfe6 at 0.05 °C of undercooling after 1 min (i) and 4 min (ii). The black bar represents a length of 50 $\mu$m.

Table 1: Ice Crystal Growth Rates in the Presence of Various Type III AFP Iisoforms, Mutants, and Mixtures[a]

| mixture | concn ($\mu$M) | growth rate ($\mu$m/min) |
|---|---|---|
| 100% SPnfe6 | 100 | 12.7 |
| 100% QAEop12 | 100 | 0 |
| 99:1 (SPnfe6 to QAEop12) | 100 | 0.3 |
| 90:10 (SPnfe6 to QAEop12) | 100 | 0.1 |
| 100% SPnfe6_P19L/A20V | 100 | 0.4 |
| 100% SPnfe6_P19L/A20V | 660 | 0.2 |
| 75:25 (SPnfe6 to SPnfe6_P19L/A20V) | 100 | 0.8 |
| 90:10 (SPnfe6 to SPnfe6_P19L/A20V) | 100 | 0.9 |
| 95:5 (SPnfe6 to SPnfe6_P19L/A20V) | 100 | 0.7 |
| 99:1 (SPnfe6 to SPnfe6_P19L/A20V) | 100 | 0.9 |

[a]All measurements were made at a temperature 0.05 °C below the equilibrium melting point of the solution.

seen in Figure 7A. At a concentration of 660 $\mu$M SPnfe6_P19L/A20V the growth rate was lowered even further to 0.2 $\mu$m/min (images not shown). However, these slow growth rates were imperceptible during TH measurements where the temperature was lowered in small increments of 0.0186 °C (10 mOsm) and growth was assessed by eye over 15 s before lowering the temperature by another increment. A distinct ice crystal burst was observed during TH measurements of SPnfe6_P19L/A20V when the nonequilibrium

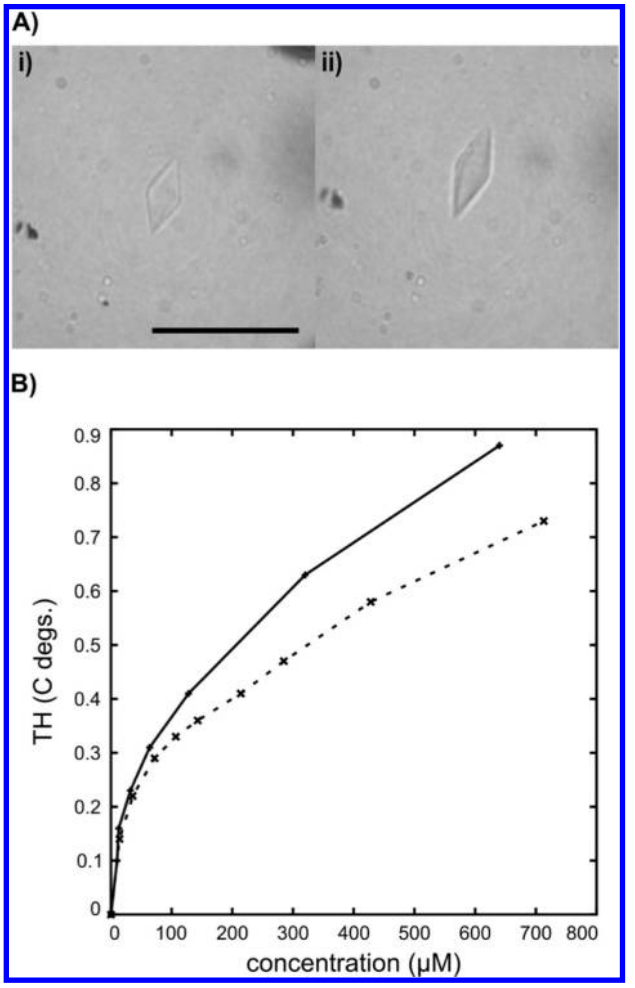


FIGURE 7: Ice crystal morphology and growth in the presence of SPnfe6_P19L/A20V. (A) Ice crystal morphology produced in a 100 $\mu$M solution of SPnfe6_P19L/A20V held 0.05 °C below the melting point after 1 min (i) and 15 min (ii). The black bar represents 50 $\mu$m. (B) Curve plotting the TH activity of SPnfe6_P19L/A20V (solid line) as a function of concentration. The TH activity of QAEop12 is also plotted for comparison (dashed line).

freezing point was exceeded, as opposed to SPnfe6 which simply allowed the crystal to grow at a faster rate when the temperature was lowered. The TH activity of the double mutant was reproducibly slightly higher than that of QAEop12, producing a typical hyperbolic curve (Figure 7B). A similar result was previously seen with some noninactivating mutants of QAEop12, specifically at R47, D58, and K61 (*32*).

*Mixing Studies of SPnfe6 with SPnfe6_P19L/A20V and QAEop12.* Although SP isoforms of type III AFP that have been tested are unable to stop ice crystal growth at undercooling temperatures (*35*, *37*), mixing small amounts of an nfe QAE isoform with SPnfe6 dramatically lowered the crystal's growth rate (*36*). Even at a ratio of 99:1 (99 $\mu$M SPnfe6 to 1 $\mu$M QAEnfe8 (an nfe QAE isoform)), the rate of growth was $^1/_{60}$th that of the growth rate produced by 100 $\mu$M SPnfe6 alone. Here we confirmed this result using small amounts of a different QAE

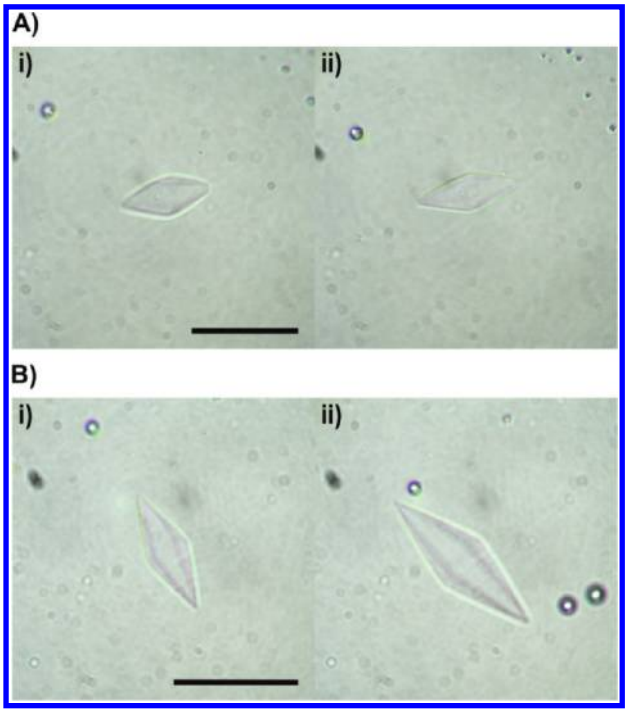


FIGURE 8: Ice crystal morphology produced by mixtures of wild-type and mutant SPnfe6 isoforms. (A) Ice crystal morphology produced in a 100 $\mu$M solution of Spnfe6:QAEop12 mixed at a ratio of 99:1 after 1 min (i) and 15 min (ii). The black bar represents 50 $\mu$m. (B) Ice crystal morphology produced in a 100 $\mu$M solution of SPnfe6:SPnfe6_P19L/A20V mixed at a ratio of 99:1 after 1 min (i) and 15 min (ii). The bar represents 50 $\mu$m.

orthologue. By mixing in 1% QAEop12 isoform (99 $\mu$M SPnfe6 to 1 $\mu$M QAEop12) the growth rate fell 40-fold from 12.7 $\mu$m/min to 0.3 $\mu$m/min (Table 1). Images of an ice crystal in the presence of the 99:1 mixture of SPnfe6:QAEop12 at 1 and 15 min are shown in Figure 8A. A 90:10 mixture of SPnfe6:QAEop12 was also tested for ice growth inhibition. The rate was lower again at 0.1 $\mu$m/min, reflecting the 10-fold increase in the ratio of QAE to SP isoforms (Table 1).

The mutation of two residues (P19L/A20V) on the surface of SPnfe6, to make it more like a QAE isoform, conferred TH activity on the protein but did not completely convert it to the wild-type activity. This was apparent from the slight growth observed when an AFP-bound ice crystal was held 0.05 °C below the equilibrium melting point. At a final concentration of 100 $\mu$M, SPnfe6_P19L/A20V slowed the growth rate from 12.7 $\mu$m/min to 0.4 $\mu$m/min (Table 1), and the growth rate was lowered even further to 0.2 $\mu$m/min at a concentration of 660 $\mu$M. Various solutions of SPnfe6 mixed with SPnfe6_P19L/A20V to a final concentration of 100 $\mu$M were tested for their ability to inhibit ice growth (Table 1). A 75:25 mixture of SPnfe6:SPnfe6_P19L/A20V resulted in ice crystals that grew at a rate of 0.8 $\mu$m/min. This growth rate was twice as fast as that produced by pure 100 $\mu$M SPnfe6_P19L/A20V but 16-fold slower than pure 100 $\mu$M SPnfe6. Three other ratios were tested (90:10, 95:5, 99:1), and they all showed roughly the same growth rate (0.8 $\mu$m/min) (Table 1). Figure 8B shows images of an ice crystal in the presence of the 99:1 mixture of SPnfe6 and SPnfe6_P19L/A20V at 1 and 15 min. While the growth of the crystal from 1 to 15 min is noticeably greater than the growth over the same period of time for the crystal in pure 100 $\mu$M SPnfe6_P19L/A20V (Figure 7A), it is still much smaller as compared to pure 100 $\mu$M SPnfe6 (Figure 6).

FIGURE 9: Traditional etch of SPnfe6. A hemisphere mounted with its secondary prism plane normal to the ice finger was grown in the presence of 0.1 mg/mL tetramethylrhodamine-labeled SPnfe6. Two distinct protein patches, oriented in the same manner as observed with GFP-SPnfe6 (Figure 3), were revealed on the surface of the crystal after the hemisphere was allowed to sublime at −20 °C for ca. 24 h. Each patch has a faint pink color resulting from the inherent fluorescence of the tetramethylrhodamine label viewed under normal light.

## DISCUSSION

*Improvement in the Ice-Etching Technique*. The ice-etching method developed by Knight et al. (*18*) has been the only dependable way to determine the plane(s) of ice to which AFPs bind. We report here a significant improvement in the method. Adding a fluorescent tag to the AFP allows for the direct visualization under UV light of bound AFP on the surface of the ice hemisphere without the need for sublimation. Also, the intensity of the fluorescent signal can be monitored at intervals during growth of the crystal. The hemisphere grown with QAEop12 fused to GFP is highly similar to the original etch of QAEop12 produced by Antson et al. (*19*) and confirms both the validity of our modification to the ice-etching method and their initial discovery that QAEop12 has affinity for more than one ice plane. The conditions we currently use for FIPA analysis are similar to those used for conventional ice etching. To illustrate this point, when an ice hemisphere grown in a solution of fluorescently labeled SPnfe6 was allowed to sublime, it produced a distinct etch (Figure 9). In this instance SPnfe6 was chemically labeled with a fluorescent tag that colored the AFP residue left on the ice surface. By increasing the intensity of fluorescent labeling and by using specific light filters, there is the potential to make FIPA more sensitive such that lower AFP concentrations and/or thinner coverage could be used.

GFP-tagged QAEop12 has been used in photobleaching experiments to demonstrate by fluorescence microscopy that no exchange occurred between bound AFP on the surface of the ice crystal and in solution (*38*). GFP-tagged AFPs (QAEop12 and sbwAFP) have also been used to demonstrate that TH hyperactivity correlates with basal plane binding (*44*). This current study and those of Pertaya et al. (*38*, *44*) demonstrate that (i) GFP does not affect the TH activity of an AFP as long as its point of attachment does not interfere with the IBS of the protein and (ii) fluorescent proteins can be used to successfully interrogate the AFP−ice interaction at both the microscopic and macroscopic levels.

*The Multi-Ice-Plane Affinity of Type III AFP*. The mechanism of action of type III AFP is clearly dependent upon it binding both primary prism and pyramidal planes. We hypothesize that these two ice planes are recognized and bound by distinct but adjacent parts of the IBS that are at an ~150° angle to each other (Figure 10). In essence, the protein surface that binds ice is a compound binding site. This introduces another

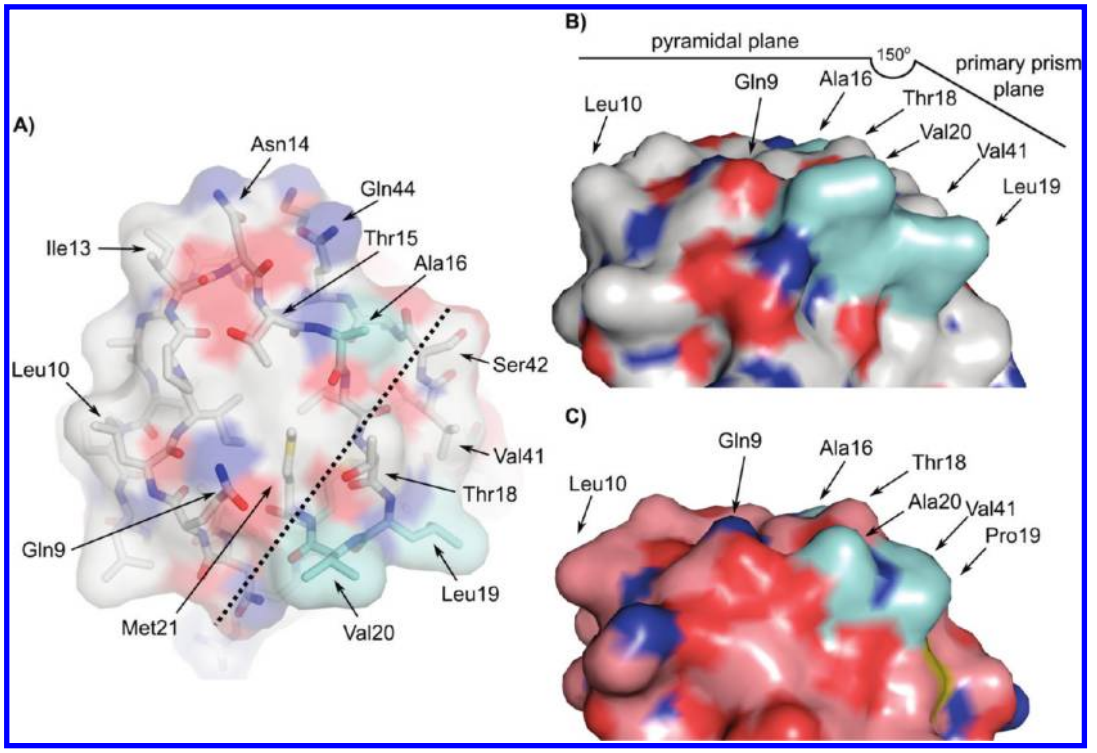


FIGURE 10: Compound IBS of QAEop12. (A) View from the top looking down onto the IBS of QAEop12 (PDB reference 1HG7). All residues involved in ice binding are labeled. The hatched line indicates the division between pyramidal plane (left of line) and primary prism plane (right of line) IBS's. Amino acids are represented as sticks with a transparent surface. Residues are colored as follows: nitrogen = blue, oxygen = red, carbon = white, and sulfur = orange. Residues shown in light blue highlight the positions of Ala16, Leu19, and Val20. (B) Surface view perpendicular to that shown in (A) of the IBS of QAEop12. The color scheme is the same as in (A). The potential primary prism and pyramidal plane binding sections of the AFP are indicated as is the angle between the two. All images in this figure were generated using the program PyMOL (http://pymol.com). (C) Equivalent surface view to that shown in (B) of the SP isoform (PDB reference 1OPS) showing key differences in the primary prism plane IBS. Carbon atoms are colored pink instead of gray.

level of complexity to what was previously thought to be a relatively simple ligand−receptor interaction (*17*) exemplified by type I AFP. This, the smallest of the AFPs, is able to prevent ice growth by binding solely to the {20−21} pyramidal plane (*18*). Even the binding of hyperactive sbwAFP to both the basal and primary prism planes is a relatively simple situation where a single IBS might fit these two planes that have common and similar spacing between O atoms (*9*). The observation that some AFPs can bind to more than one structurally distinct plane of ice explains why it has been extremely difficult to knock down the activity of the moderately active type II AFP (*13*, *45*) and why fluorescently tagged hyperactive snow flea AFP binds uniformly over the entire surface of a single-crystal hemisphere (*46*).

Our results show that even with multi-ice-plane affinity, an AFP can remain moderately active. Scotter et al. (*42*) demonstrated that the key to hyperactivity for an AFP is the ability to bind the basal plane of ice in addition to other specific planes. The etches obtained with both type III and type I clearly show no basal plane binding. This leaves ice crystals in the presence of these AFPs susceptible to growth out of the uncovered tips of the hexagonal bipyramids (*47*), limiting their antifreeze activity as compared to hyperactive AFPs.

*The Compound Ice-Binding Site of Type III AFP*. The presence of a compound IBS in type III AFP helps to explain how certain mutations on the IBS alter the protein's affinity toward specific planes of ice. Deluca et al. (*43*) showed that substituting Ala16 for His on QAEop12 (which lies at one edge of the pyramidal plane-binding IBS (Figure 10B) but close to the boundary between the two adjacent IBSs) resulted in TH levels that were reduced to 25% of wild-type activity and produced ice crystals with a greater *c*:*a* axis ratio. The fluorescent hemisphere obtained with this mutant showed that it predominantly binds to the primary prism plane of ice having lost the wild-type's ability to also bind a pyramidal plane. The lack of pyramidal plane binding could logically result in ice crystals with an extended *c*:*a* axis ratio as the mutant protein's ability to taper the ice crystal into a hexagonal bipyramid might be hindered. Even the simple act of diluting the wild-type QAE isoform resulted in elongated crystals with a higher *c*:*a* axis ratio. This would be consistent with the different halves of the compound IBS having different rates of association with their respective ice planes.

Takamichi et al. (*36*) showed that SPnfe6 was able to shape ice into hexagonal bipyramids typical of type III AFP but was unable to prevent their growth during situations of undercooling. The fluorescent hemisphere obtained with this mutant (Figure 3) showed SPnfe6 bound mainly to a pyramidal plane of ice while its ability to bind the primary prism plane of ice was severely attenuated. Although SPnfe6 is only 58% identical with QAEop12 at the amino acid level, the residues that constitute the compound IBS are conserved between the two proteins, except at positions 19 and 20 (Leu and Val in QAEop12, Pro and Ala in SPnfe6, respectively). SPnfe6 can therefore be viewed as a double IBS mutant of QAEop12.

The compound IBS of type III AFP is composed of a dozen residues located in a relatively hydrophobic area of the protein (*24*, *25*, *28*−*30*, *32*, *33*) (Figure 10A). These include Gln9, Leu10, Ile13, Asn14, Thr15, Ala16, Thr18, Leu19, Val20, Met21, Val41, and Gln44. Of these residues, we suggest that Thr18, Leu19, Val20, and Val41 constitute the primary prism plane IBS. This IBS is inclined at a −30° angle to the pyramidal plane IBS

and is also flat and relatively hydrophobic (Figure 10B). We think that the remaining residues are responsible for docking the protein to a pyramidal plane of ice. Baardsnes and Davies (*28*) showed that making hydrophobic residues smaller on or around the IBS of the protein resulted in significant decreases in the TH activity. In particular, individual Ala substitutions at residues Leu19 and Val20 each resulted in a 23% loss of TH activity as compared to the wild type. The hemisphere pattern obtained with SPnfe6 showed that these two residues play a critical role in docking the protein to the primary prism plane of ice. Loss of binding to this plane causes the ice crystal to grow but with the same *c*- to *a*-axial ratio as the wild type. Changing SPnfe6 into a more "QAE-like" type III AFP isoform by making the double P19L/A20V substitution restored near wild-type TH levels but did not affect the ice crystal morphology.

*Do Other AFP Gene Families Show Cooperativity between Isoforms?* Most AFPs are members of multigene families (*48*, *49*), and type III AFP is an excellent example of this phenomenon. The beetle *Dendroides canadensis* also produces a family of several different AFP isoforms, four of which reside in the hemolymph of the insect (*50*). These four isoforms are able to significantly enhance the TH activity of one another, especially when all four are mixed together at equimolar amounts. The exact mechanism of this enhancement remains elusive, however. It is possible that these individual isoforms are able to bind different planes of ice and that maximal TH levels are produced only when all four are combined, providing greater surface coverage of the ice crystal. The amino acid differences between these isoforms are minimal, yet as was demonstrated in this paper, only two mutations are required to drastically alter the ice-binding ability of an AFP. Tagging these individual beetle hemolymph isoforms with GFP and performing FIPA analysis would go a long way in deciphering the mechanism of action of this enhancement.

*The TH Activity of Spnfe6_P19L/A20V*. The TH activity of SPnfe6_P19L/A20V was consistently slightly higher (ca. 20%) than QAEop12. While the double mutant was unable to completely inhibit ice growth, growth was undetectable when lowering the temperature of the solution at a rate of 10 mOsm every 15 s, the standard rate for TH measurements on moderately active AFPs. If, between temperature reductions, no change in ice shape or size is detectable, then the end point of the TH measurement has not yet been reached. The fast rate of growth of ice crystals in the presence of wild-type SPnfe6 is apparent from the start of TH measurements, making it clear that this isoform is unable to stop ice growth. Also, ice crystals in the presence of the double mutant distinctly burst out the tips once the nonequilibrium freezing point was exceeded, whereas the burst point for SPnfe6 was extremely difficult to determine in most instances.

SPnfe6_P19L/A20V decreased ice crystal growth rates by at least 14-fold as compared to pure SPnfe6 when mixed at a ratio of 1:99 with SPnfe6. A 60-fold decrease in the growth rate was reported when mixing SPnfe6 with QAEnfe8 (a naturally occurring QAE isoform produced by the notched fin eelpout) at a 99:1 ratio (*36*). This implies that while P19L and A20V make SPnfe6 much more QAE-like, there must be one or more other residues that will have to be changed to make this isoform equivalent to wild-type QAE isoform.

In conclusion, a significant improvement in the technique of growing and interpreting AFP-bound macromolecular single-crystal ice hemispheres has been accomplished through the use of fluorescently tagged AFPs. This has allowed for the visualization of the AFP−ice interaction under UV light. By fusing GFP to wild-type and mutant QAE and SP isoforms of type III AFP, the improved technique confirmed that type III AFP is able to bind multiple planes of ice, including both the primary prism plane and a pyramidal plane. This analysis has revealed that type III AFP, and likely many other AFPs, has compound ice-binding sites, parts or all of which can bind the protein to different planes of ice.

## ACKNOWLEDGMENT

We thank Dr. Rob Campbell for comments on the manuscript.

## REFERENCES

1. Duman, J. G., Bennett, V., Sformo, T., Hochstrasser, R., and Barnes, B. M. (2004) Antifreeze proteins in Alaskan insects and spiders. *J. Insect Physiol. 50*, 259–266.
2. Duman, J. G., and Olsen, T. M. (1993) Thermal hysteresis protein activity in bacteria, fungi and phylogenetically diverse plants. *Cryobiology 30*, 322–328.
3. Fletcher, G. L., Hew, C. L., and Davies, P. L. (2001) Antifreeze proteins of teleost fishes. *Annu. Rev. Physiol. 63*, 359–390.
4. Raymond, J. A., and DeVries, A. L. (1977) Adsorption inhibition as a mechanism of freezing resistance in polar fishes. *Proc. Natl. Acad. Sci. U.S.A. 74*, 2589–2593.
5. Knight, C. A., and Devries, A. L. (1989) Melting inhibition and superheating of ice by an antifreeze glycopeptide. *Science 245*, 505–507.
6. Celik, Y., Graham, L. A., Mok, Y. F., Bar, M., Davies, P. L., and Braslavsky, I. (2009) Superheating of ice crystals in antifreeze protein solutions. *Proc. Natl. Acad. Sci. U.S.A. 107*, 5423–5428.
7. Kristiansen, E., and Zachariassen, K. E. (2005) The mechanism by which fish antifreeze proteins cause thermal hysteresis. *Cryobiology 51*, 262–280.
8. Garnham, C. P., Gilbert, J. A., Hartman, C. P., Campbell, R. L., Laybourn-Parry, J., and Davies, P. L. (2008) A $Ca^{2+}$-dependent bacterial antifreeze protein domain has a novel beta-helical ice-binding fold. *Biochem. J. 411*, 171–180.
9. Graether, S. P., Kuiper, M. J., Gagne, S. M., Walker, V. K., Jia, Z., Sykes, B. D., and Davies, P. L. (2000) Beta-helix structure and ice-binding properties of a hyperactive antifreeze protein from an insect. *Nature 406*, 325–328.
10. Ko, T. P., Robinson, H., Gao, Y. G., Cheng, C. H., DeVries, A. L., and Wang, A. H. (2003) The refined crystal structure of an eel pout type III antifreeze protein RD1 at 0.62-Å resolution reveals structural microheterogeneity of protein and solvation. *Biophys. J. 84*, 1228–1237.
11. Liou, Y. C., Tocilj, A., Davies, P. L., and Jia, Z. (2000) Mimicry of ice structure by surface hydroxyls and water of a beta-helix antifreeze protein. *Nature 406*, 322–324.
12. Liu, Y., Li, Z., Lin, Q., Kosinski, J., Seetharaman, J., Bujnicki, J. M., Sivaraman, J., and Hew, C. L. (2007) Structure and evolutionary origin of $Ca^{2+}$-dependent herring type II antifreeze protein. *PLoS ONE 2*, e548.
13. Nishimiya, Y., Kondo, H., Takamichi, M., Sugimoto, H., Suzuki, M., Miura, A., and Tsuda, S. (2008) Crystal structure and mutational analysis of $Ca^{2+}$-independent type II antifreeze protein from long-snout poacher, *Brachyopsis rostratus*. *J. Mol. Biol. 382*, 734–746.
14. Pentelute, B. L., Gates, Z. P., Tereshko, V., Dashnau, J. L., Vanderkooi, J. M., Kossiakoff, A. A., and Kent, S. B. (2008) X-ray structure of snow flea antifreeze protein determined by racemic crystallization of synthetic protein enantiomers. *J. Am. Chem. Soc. 130*, 9695–9701.
15. Sicheri, F., and Yang, D. S. (1995) Ice-binding structure and mechanism of an antifreeze protein from winter flounder. *Nature 375*, 427–431.
16. Davies, P. L., Baardsnes, J., Kuiper, M. J., and Walker, V. K. (2002) Structure and function of antifreeze proteins. *Philos. Trans. R. Soc. London, Ser. B 357*, 927–935.
17. Jia, Z., and Davies, P. L. (2002) Antifreeze proteins: an unusual receptor-ligand interaction. *Trends Biochem. Sci. 27*, 101–106.
18. Knight, C. A., Cheng, C. C., and DeVries, A. L. (1991) Adsorption of alpha-helical antifreeze peptides on specific ice crystal surface planes. *Biophys. J. 59*, 409–418.
19. Antson, A. A., Smith, D. J., Roper, D. I., Lewis, S., Caves, L. S., Verma, C. S., Buckley, S. L., Lillford, P. J., and Hubbard, R. E. (2001) Understanding the mechanism of ice binding by type III antifreeze proteins. *J. Mol. Biol. 305*, 875–889.

20. Knight, C. A., and DeVries, A. L. (1988) The prevention of ice crystal growth from water by "antifreeze protein", in Atmospheric Aerosol and Nucleation (Wagner, P. E., and Valli, G., Eds.) pp 717−720, Springer, Berlin.
21. Cheng, C. C., and DeVries, A. L. (1991) The role of antifreeze glycopeptides and peptides in the freezing avoidance of cold-water fish, in Life Under Extreme Conditions (di Prisco, G., Ed.) pp 1−14, Springer-Verlag, Berlin.
22. Schrag, J. D., Cheng, C. H., Panico, M., Morris, H. R., and DeVries, A. L. (1987) Primary and secondary structure of antifreeze peptides from arctic and antarctic zoarcid fishes. *Biochim. Biophys. Acta 915*, 357–370.
23. Hew, C. L., Wang, N. C., Joshi, S., Fletcher, G. L., Scott, G. K., Hayes, P. H., Buettner, B., and Davies, P. L. (1988) Multiple genes provide the basis for antifreeze protein diversity and dosage in the ocean pout, *Macrozoarces americanus*. *J. Biol. Chem. 263*, 12049–12055.
24. Jia, Z., DeLuca, C. I., Chao, H., and Davies, P. L. (1996) Structural basis for the binding of a globular antifreeze protein to ice. *Nature 384*, 285–288.
25. Sonnichsen, F. D., DeLuca, C. I., Davies, P. L., and Sykes, B. D. (1996) Refined solution structure of type III antifreeze protein: hydrophobic groups may be involved in the energetics of the protein-ice interaction. *Structure 4*, 1325–1337.
26. Sonnichsen, F. D., Sykes, B. D., Chao, H., and Davies, P. L. (1993) The nonhelical structure of antifreeze protein type III. *Science 259*, 1154–1157.
27. Yang, D. S., Hon, W. C., Bubanko, S., Xue, Y., Seetharaman, J., Hew, C. L., and Sicheri, F. (1998) Identification of the ice-binding surface on a type III antifreeze protein with a "flatness function" algorithm. *Biophys. J. 74*, 2142–2151.
28. Baardsnes, J., and Davies, P. L. (2002) Contribution of hydrophobic residues to ice binding by fish type III antifreeze protein. *Biochim. Biophys. Acta 1601*, 49–54.
29. Chao, H., Sonnichsen, F. D., DeLuca, C. I., Sykes, B. D., and Davies, P. L. (1994) Structure-function relationship in the globular type III antifreeze protein: identification of a cluster of surface residues required for binding to ice. *Protein Sci. 3*, 1760–1769.
30. DeLuca, C. I., Chao, H., Sonnichsen, F. D., Sykes, B. D., and Davies, P. L. (1996) Effect of type III antifreeze protein dilution and mutation on the growth inhibition of ice. *Biophys. J. 71*, 2346–2355.
31. DeLuca, C. I., Davies, P. L., Ye, Q., and Jia, Z. (1998) The effects of steric mutations on the structure of type III antifreeze protein and its interaction with ice. *J. Mol. Biol. 275*, 515–525.
32. Graether, S. P., DeLuca, C. I., Baardsnes, J., Hill, G. A., Davies, P. L., and Jia, Z. (1999) Quantitative and qualitative analysis of type III antifreeze protein structure and function. *J. Biol. Chem. 274*, 11842–11847.
33. Siemer, A. B., and McDermott, A. E. (2008) Solid-state NMR on a type III antifreeze protein in the presence of ice. *J. Am. Chem. Soc. 130*, 17394–17399.
34. Yang, C., and Sharp, K. A. (2004) The mechanism of the type III antifreeze protein action: a computational study. *Biophys. Chem. 109*, 137–148.
35. Nishimiya, Y., Sato, R., Takamichi, M., Miura, A., and Tsuda, S. (2005) Co-operative effect of the isoforms of type III antifreeze protein expressed in Notched-fin eelpout, *Zoarces elongatus* Kner. *FEBS J. 272*, 482–492.
36. Takamichi, M., Nishimiya, Y., Miura, A., and Tsuda, S. (2009) Fully active QAE isoform confers thermal hysteresis activity on a defective SP isoform of type III antifreeze protein. *FEBS J. 276*, 1471–1479.
37. Kenward, K. D. (1995) Expression of fish antifreeze protein genes in transgenic tobacco for increased plant freeze resistance and as a model for molecular farming, Ph.D. Thesis, Department of Biochemistry, Queen's University, Kingston, Ontario, Canada.
38. Pertaya, N., Marshall, C. B., DiPrinzio, C. L., Wilen, L., Thomson, E. S., Wettlaufer, J. S., Davies, P. L., and Braslavsky, I. (2007) Fluorescence microscopy evidence for quasi-permanent attachment of antifreeze proteins to ice surfaces. *Biophys. J. 92*, 3663–3673.
39. Chao, H., Davies, P. L., Sykes, B. D., and Sonnichsen, F. D. (1993) Use of proline mutants to help solve the NMR solution structure of type III antifreeze protein. *Protein Sci. 2*, 1411–1428.
40. Knight, C. A. (1966) Formation of crystallographic etch pits on ice, and its application to the study of hailstones. *J. Appl. Meteorol. 5*, 710–714.
41. Chakrabartty, A., and Hew, C. L. (1991) The effect of enhanced alpha-helicity on the activity of a winter flounder antifreeze polypeptide. *Eur. J. Biochem. 202*, 1057–1063.
42. Scotter, A. J., Marshall, C. B., Graham, L. A., Gilbert, J. A., Garnham, C. P., and Davies, P. L. (2006) The basis for hyperactivity of antifreeze proteins. *Cryobiology 53*, 229–239.
43. DeLuca, C. I., Comley, R., and Davies, P. L. (1998) Antifreeze proteins bind independently to ice. *Biophys. J. 74*, 1502–1508.
44. Pertaya, N., Marshall, C. B., Celik, Y., Davies, P. L., and Braslavsky, I. (2008) Direct visualization of spruce budworm antifreeze protein interacting with ice crystals: basal plane affinity confers hyperactivity. *Biophys. J. 95*, 333–341.
45. Loewen, M. C., Gronwald, W., Sonnichsen, F. D., Sykes, B. D., and Davies, P. L. (1998) The ice-binding site of sea raven antifreeze protein is distinct from the carbohydrate-binding site of the homologous C-type lectin. *Biochemistry 37*, 17745–17753.
46. Mok, Y. F., Lin, F. H., Graham, L. A., Celik, Y., Braslavsky, I., and Davies, P. L. (2010) Structural basis for the superior activity of the large isoform of snow flea antifreeze protein. *Biochemistry 49*, 2593–2603.
47. Knight, C. A., and DeVries, A. L. (2009) Ice growth in supercooled solutions of a biological "antifreeze", AFGP 1−5: an explanation in terms of adsorption rate for the concentration dependence of the freezing point. *Phys. Chem. Chem. Phys. 11*, 5749–5761.
48. Graham, L. A., Qin, W., Lougheed, S. C., Davies, P. L., and Walker, V. K. (2007) Evolution of hyperactive, repetitive antifreeze proteins in beetles. *J. Mol. Evol. 64*, 387–398.
49. Swanson, W. J., and Aquadro, C. F. (2002) Positive darwinian selection promotes heterogeneity among members of the antifreeze protein multigene family. *J. Mol. Evol. 54*, 403–410.
50. Wang, L., and Duman, J. G. (2005) Antifreeze proteins of the beetle *Dendroides canadensis* enhance one another's activities. *Biochemistry 44*, 10305–10312.